

# A stress-function variational approach toward CFRP -concrete interfacial stresses in bonded joints

Hojjat Samadvand<sup>a</sup> and Mehdi Dehestani\*

Department of Civil Engineering, Babol Noshirvani University of Technology, Babol, Iran

(Received July 21, 2018, Revised September 29, 2019, Accepted October 15, 2019)

**Abstract.** This paper presents an innovative stress-function variational approach in formulating the interfacial shear and normal stresses in an externally bonded concrete joint using carbon fiber-reinforced plastic (CFRP) plies. The joint is subjected to surface traction loadings applied at both ends of the concrete substrate layer. By introducing two interfacial shear and normal stress functions on the CFRP-concrete interface, based on Euler-Bernoulli beam idea and static stress equations of equilibrium, the entire stress fields of the joint were determined. The complementary strain energy was minimized in order to solve the governing equation of the joint. This yields an ordinary differential equation from which the interfacial normal and shear stresses were proposed explicitly, satisfying all the multiple traction boundary conditions. Lamination theory for composite materials was also employed to obtain the interfacial stresses. The proposed approach was validated by the analytic models in the literature as well as through a comprehensive computational code generated by the authors. Furthermore, a numerical verification was carried out via the finite element software ABAQUS. In the end, a scaling analysis was conducted to analyze the interfacial stress field dependence of the joint upon effective issues using the devised code.

**Keywords:** interfacial stress; bonded joint; CFRP composite; concrete; lamination theory

## 1. Introduction

Over the last three decades, there has been an increasing understanding of the unique features of advanced FRP composites among civil engineers and the construction industry. Today, designers opt for fibrous composites for a range of reasons such as low weight, high stiffness and strength, electrical conductivity (or nonconductivity), low thermal expansion, low/high rate of heat transfer, corrosion resistance, longer fatigue life, optimal design, reduced maintenance, retaining properties at high temperatures, etc. (Herakovich 1998). The applications will expand even faster as better and more economical composites are introduced, and as more engineers become knowledgeable in the analysis, design, and fabrication of such composites (Herakovich 1998). Considering the fact that monolithic metals and manufactured alloys are not sufficient for the present advanced technologies, one can meet the performance requirements solely by combining several materials together. This leaves composites as the only materials to satisfy such demands (Kaw 2006). In many cases, the strengthening of concrete structures seems to be essential owing to different reasons including design or construction errors, change in structural application, steel corrosion, concrete chemical degradation, modification of codes and standards, and structural damage caused by

natural disasters or accidents. As a result, FRP materials have been introduced as an acceptable implement in the retrofitting, repairing and enhancing the service life of existing structures as well as in creating new ones. Moreover, a wide range of methods has been developed in joining structural parts together, two of which are the mechanical fastening and adhesive bonding, where the latter excels in different aspects. Researches have revealed that externally bonding of FRP sheet with epoxy resin is an efficient procedure for strengthening and repairing reinforced concrete (RC) beams under flexural loads (Hashemi *et al.* 2008).

It has been well established that the adhesively bonded members are lighter, more fatigue resistant, easily handled, and rapidly implemented (Pattabhi *et al.* 2012). Besides, in this method, the area of interest is strengthened without change in the structure's stiffness or disturbance of the architecture; thus the use of advanced FRP composites applied to structural members as externally bonded reinforcement has come to prominence in the retrofitting technology (Karbhari and Abanilla 2007).

Researches in the recent years represent the fact that obtaining higher load-bearing capacity of concrete elements retrofitted with FRP composites, would be unattainable due to some parametric effects embracing FRP debonding failure prior to reaching the ultimate stresses. This, in turn, is greatly affected by the high interfacial stresses near the free edges of such elements. However, concrete crushing, FRP rupture, shear failure (Hosseini and Mostofinejad 2013), concrete cover separation failure (Smith and Teng 2002a, Smith and Teng 2002b, Smith and Teng 2003), plate end interfacial debonding (Smith and Teng 2002a, Smith and Teng 2002b, Oehlers and Moran 1990), critical

\*Corresponding author, Associate Professor

E-mail: [dehestani@nit.ac.ir](mailto:dehestani@nit.ac.ir)

<sup>a</sup>Graduate Student

E-mail: [Samadvand@gmail.com](mailto:Samadvand@gmail.com)

diagonal crack debonding (CDC) (Ali *et al.* 2001, Ali *et al.* 2002, Oehlers *et al.* 2003) and interfacial debonding due to intermediate crack (IC) (Teng *et al.* 2003) are the numerous modes of failure in externally strengthened concrete members which make the joint analysis more complicated. In this context, Dogan and Anil (2010) employed a numerical finite element model to find the stress distribution, load-displacement behavior, and CFRP bonding length as well as the strain field along concrete-CFRP interface. They then reported a good agreement between the modelling results and those obtained from experiments.

High interfacial stresses along the bondline, particularly close to edges, exist due to mismatch in Poisson's ratios and coefficients of mutual influence of adherents. Therefore, a careful study on the interfacial properties of concrete joints strengthened with FRP, as well as the analysis of affecting parameters would be indispensable. Considerable attention has been paid by the research community to understand the mechanical behavior and durability of such joints, either analytically or numerically. Puppo and Evensen (1970) proposed a finite width composite laminate solution based on a model with anisotropic lamina and isotropic shear layers with interlaminar normal stress being neglected. Pagano (Pagano 1978a, Pagano 1978b) developed an appropriate theory based on Reissner's variational principle. The stresses were assumed to be in-plane and there was no stress singularity in the formulation. Pipes and Pagano (1974) presented an approximate elasticity solution to calculate the stress fields at straight free-edges of composite laminates. Tang (1975), Tang and Levy (1975) developed a boundary layer theory to determine such stresses. Kassapoglou and Lagace (1986, 1987), outlined a simple technique in the analysis of symmetrical laminates. They used the principal of minimum complementary energy method for laminates under tension/compression loadings. The approach was later extended by Kassapoglou (1990) for asymmetric laminates under combined in-plane loadings. However, it didn't model the through-thickness mismatch in Poisson's ratios and the coefficients of mutual influence of the adjoining layers. Wu and Dzenis (2005) experimentally determined the edge delamination of FRP/epoxy composite via stress-function variational approach. Wu and Jenson (2011) proposed a stress-function variational method which could accurately predict interfacial stresses. In another work, Wu and Jenson (2014) reported a semi-analytic approach to determine the interfacial shear and normal stresses in a steel-aluminum bimaterial bonded joint under mechanical and thermal loads. Touati *et al.* (2015) employed an analytical approach in finding adhesive stresses in a concrete beam bonded with the FRP plate, considering the effect of adherend shear deformations. Khan *et al.* (2017) numerically investigated shear behavior of RC beams strengthened with CFRP sheets and reported that proper modelling of bond behavior of interfaces is of significant importance in the shear behavior of such beams. Fracture of CFRP-concrete composite bonded interfaces was recently considered by Lin *et al.* (2017). The presented fracture models demonstrated that the fracture behavior depends on the relative interfacial cohesive strength, as well as the concrete tensile strength.

In addition to the aforementioned efforts, extensive research has led to the existing design guidelines to be published worldwide such as the American Concrete Institute (ACI) 2008; International Federation for Structural Concrete (fib) 2001; Japan Society of Civil Engineers (JSCE) 2001; National Council of Research (CNR) 2004, and Concrete Society 2004.

### 1.1 Research significance

A good number of researches have been conducted so far to investigate the stress fields at the bondline, however, these models have been oversimplified in different aspects. Firstly, some are limited to the prediction of interlaminar stresses at the body of laminated FRP-composite plates and shells, rather than considering interfacial stresses on the concrete-FRP surface (delamination rather than debonding); whereas proper selection of strengthening materials can considerably postpone or totally eliminate delamination failure. Secondly, they do not precisely satisfy the boundary conditions at free edges of the joints. While free edges of bonded layers are supposed to be shear-free, these models declare that the maximum shear stresses happen at free edge of the bondline. The present study extends the recently developed (Wu and Jenson 2014) stress-function variational method in order to accurately and explicitly determine the stress fields in CFRP-concrete interface. In addition to accuracy, the proposed approach has two further advantages: not only does it satisfy the shear-free conditions of free edges of the bondline, it can also be easily generalized to joints with different geometries and loading configurations, providing a framework for further investigations.

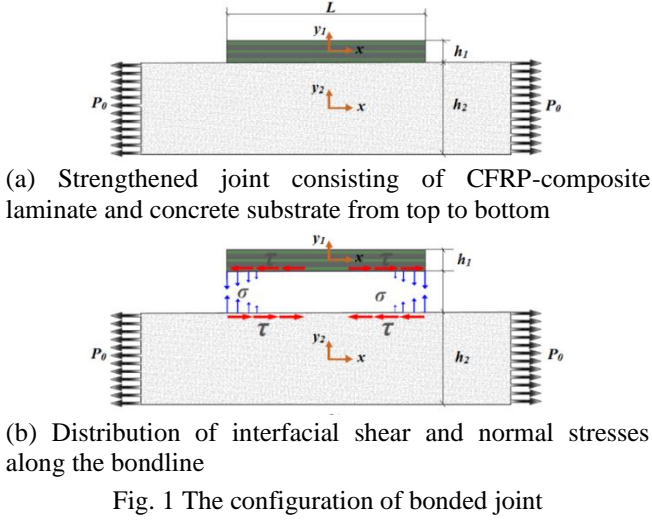
## 2. Problem formulation

### 2.1 Overview

In this section, a systematic extension of the stress-function variational approach is clarified in order to express the interfacial shear and normal stresses in a concrete substrate reinforced with a CFRP laminate composite cover. The proposed stress fields will be validated via a robust, efficient MATLAB code, based on the fundamentals of lamination theory and through comparison with the existing analytic models in the literature as well as the FEM. To be precise, the interfacial stress fields are in 3D state at free edges of the bondline. However, to simplify the process of analysis, the joint is considered to be in plane-stress state.

### 2.2 Model formulation

The configuration of a simply supported concrete prism strengthened with CFRP-composite cover along with interfacial shear and normal stress distributions are shown in Fig. 1 (a)-(b). The joint consists of cover layer (CFRP-composite laminate) and the substrate layer (concrete prism) from top to bottom with a uniform width  $b$  and an overlap bonding length  $L$ . Thickness of the CFRP-composite laminate and concrete prism are  $h_1$  and  $h_2$ ,



respectively. The thickness of CFRP-composite layers are considered to be equal. The coordinate system is considered from the symmetric mid-span of the joint; the  $x$ -axis is selected in the centroid of cross sections of each adherent along the respective layer axis;  $y_1$  and  $y_2$  are the vertical coordinates of CFRP-composite laminate and concrete prism, respectively. The stacking sequence of plies in CFRP-composite laminate is  $[0/90]$ , which denotes fiber orientation of 0 and 90 degrees with respect to  $x$ -axis from bottom to top. The external loading can include axial tension, bending moment, shear traction, temperature change, hygroscopic loading or a combination of them. The joint under study, is subjected to a uniform tensile traction  $P_0$  at both ends of concrete substrate and far enough from the bondline, so that the effects of stress concentrations can be ignored. Since the joint is not laterally symmetric, lateral deflection is probable in addition to in-plane elongation. The concrete prism is considered to be isotropic and the CFRP-composite layers are treated as transversely isotropic. It is assumed that no slip takes place between layers.

### 2.3 Static equations of equilibrium

Fig. 2 (a)-(b) illustrates typical representative elements of CFRP cover and concrete substrate together with stress resultants, which comply the conventional sign standards (Beer *et al.* 2009). For the representative element of strengthening cover (Fig. 2(a)), the static equations of equilibrium read

$$\sum F_x = 0: \frac{dN_1}{dx} = -\tau b \quad (1)$$

$$\sum F_y = 0: \frac{dQ_1}{dx} = -\sigma b \quad (2)$$

$$\sum M = 0: \frac{dM_1}{dx} = Q_1 - \frac{\tau h_1 b}{2} \quad (3)$$

Meanwhile, the relevant equilibrium equations for the representative segmental element of concrete substrate are

$$\sum F_x = 0: \frac{dN_2}{dx} = \tau b \quad (4)$$

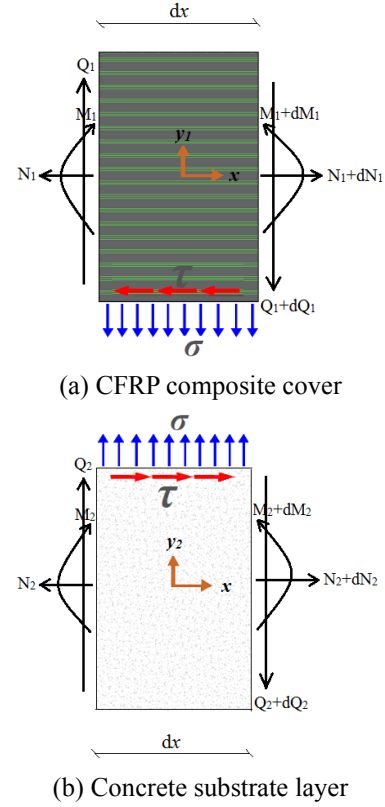


Fig. 2 Free-body diagrams of representative segmental elements of the adherents

$$\sum F_y = 0: \frac{dQ_2}{dx} = \sigma b \quad (5)$$

$$\sum M = 0: \frac{dM_2}{dx} = Q_2 - \frac{\tau h_2 b}{2} \quad (6)$$

### 2.4 Stress resultants

Two unknown stress functions are introduced as  $\tau = \psi(x)$  and  $\sigma = \phi(x)$  to represent the interfacial normal and shear stresses. Since the joint is symmetric with respect to  $y$ -axis, the shear stress function  $\psi(x)$  and the normal stress function  $\phi(x)$  are to be odd and even functions, respectively.

Furthermore, the  $x$ -axis is aligned horizontally, so that the two unknowns are expressed as functions of variable  $x$ . The shear stress at free edges of the bondline,  $x = -L/2$  and  $x = +L/2$  requires that the interfacial shear stress function be zero.

By integrating of Eq. (1) regarding  $x$  from  $x = -L/2$  and applying the physical condition at  $x = -L/2$ , i.e.,  $N_1(-L/2) = 0$ , the normal stress resultant is given by

$$N_1(x) = -b \int_{-L/2}^x \psi(\xi) d\xi \quad (7)$$

At the same time, integration of the Eqs. (2)-(3) with respect to  $x$  from  $x = -L/2$  along with applying the associated boundary conditions, i.e.,  $Q_1(-L/2) = 0$ , and

$M_1(-L/2) = 0$ , give

$$Q_1(x) = -b \int_{-L/2}^x \phi(\xi) d\xi \quad (8)$$

$$M_1(x) = -b \int_{-L/2}^x \int_{-L/2}^{\xi} \phi(\eta) d\eta d\xi - \frac{h_1 b}{2} \int_{-L/2}^x \psi(\xi) d\xi \quad (9)$$

The same trend is used for the stress resultants of concrete substrate by integration of the Eqs. (4)-(6) with respect to  $x$  from  $x = -L/2$  and taking into account the relevant boundary conditions, i.e.,  $N_2(-L/2) = P_0 b h_2$ ,  $Q_2(-L/2) = 0$  and  $M_2(-L/2) = 0$ , for the traction, shear and moment, respectively. The axial traction  $N_2(x)$ , shear force  $Q_2(x)$  and bending moment  $M_2(x)$ , can be simply computed as

$$N_2(x) = P_0 b h_2 + b \int_{-L/2}^x \psi(\xi) d\xi \quad (10)$$

$$Q_2(x) = b \int_{-L/2}^x \phi(\xi) d\xi \quad (11)$$

$$M_2(x) = b \int_{-L/2}^x \int_{-L/2}^{\xi} \phi(\eta) d\eta d\xi - \frac{h_2 b}{2} \int_{-L/2}^x \psi(\xi) d\xi \quad (12)$$

In order to correlate the interfacial shear  $\psi(x)$  and normal  $\phi(x)$  stress functions along the interface, as well as to simplify the calculations, the deformation compatibility is used in a way that the radii of curvature of CFRP-composite laminate and the concrete substrate layer are assumed to be approximately the same

$$\frac{1}{\rho_1} = \frac{1}{\rho_2} \equiv \frac{M_1}{E_1 I_1} = \frac{M_2}{E_2 I_2} \quad (13)$$

where  $I_1 = 1/12 b h_1^3$  and  $I_2 = 1/12 b h_2^3$  are moments of inertia of CFRP laminate and concrete layer, respectively. Hence, substituting from (9) and (12) into (13), it yields

$$\begin{aligned} & -\frac{E_2}{E_1} \left(\frac{h_2}{h_1}\right)^3 \left[ \int_{-L/2}^x \int_{-L/2}^{\xi} \phi(\eta) d\eta d\xi - \frac{h_1}{2} \int_{-L/2}^x \psi(\xi) d\xi \right] \\ & = \int_{-L/2}^x \int_{-L/2}^{\xi} \phi(\eta) d\eta d\xi - \frac{h_2}{2} \int_{-L/2}^x \psi(\xi) d\xi \end{aligned} \quad (14)$$

By performing a differentiation of Eq. (14) and defining the parameters as  $e_{21} = E_2/E_1$ ,  $h_{21} = h_2/h_1$  and  $\eta_0 = e_{21} h_{21}^3 + 1/(e_{21} h_{21}^2 - 1)$ , Eq. (14) can be reduced to

$$\psi(x) = -2 \frac{\eta_0}{h_2} \int_{-L/2}^x \phi(\xi) d\xi \quad (15)$$

Accordingly, the bending moments in Eqs. (9)-(12) become

$$M_1(x) = -\frac{h_1 b}{2} (1 - \eta_0^{-1} h_{21}) \int_{-L/2}^x \psi(\xi) d\xi \quad (16)$$

$$M_2(x) = -\frac{h_2 b}{2} (1 + \eta_0^{-1}) \int_{-L/2}^x \psi(\xi) d\xi \quad (17)$$

## 2.5 Stress components

According to conventional Euler-Bernoulli beam concept, axial normal stress of the CFRP-composite laminate is as follows

$$\sigma_{xx}^{(1)} = \frac{N_1}{h_1 b} - \frac{M_{1y_1}}{I_1} = \left[ -\frac{1}{h_1} + \frac{6y_1}{h_1^2} (1 - \eta_0^{-1} h_{21}) \right] \int_{-L/2}^x \psi(\xi) d\xi \quad (18)$$

Besides, integrating the 2D static equilibrium equation

$$\frac{\partial \sigma_{xx}^{(1)}}{\partial x} + \frac{\partial \tau_{y_1 x}^{(1)}}{\partial y_1} = 0 \quad (19)$$

with respect to  $y_1$  from an arbitrary point to the top surface  $y_1 = h_1/2$  and considering the physical condition  $\tau_{y_1 x}^{(1)}(h_1/2) = 0$ , the shear stress  $\tau_{y_1 x}^{(1)} = \tau_{x y_1}^{(1)}$  of the CFRP cover layer is

$$\tau_{y_1 x}^{(1)} = \left[ -\frac{1}{h_1} \left( \frac{h_1}{2} - y_1 \right) + \frac{3}{h_1^2} \left( \frac{h_1^2}{4} - y_1^2 \right) (1 - \eta_0^{-1} h_{21}) \right] \psi(x) \quad (20)$$

In addition, the normal stress  $\sigma_{yy}^{(1)}$  of the CFRP-composite laminate is expressed based on the equilibrium equation

$$\frac{\partial \sigma_{yy}^{(1)}}{\partial y_1} + \frac{\partial \tau_{xy_1}^{(1)}}{\partial x} = 0 \quad (21)$$

relative to  $y_1$  from the upper face  $y_1 = h_1/2$  which reads

$$\begin{aligned} \sigma_{yy}^{(1)} = & - \left[ \frac{1}{h_1} \left( \frac{h_1}{2} - \left( \frac{h_1^2}{8} - \frac{y_1^2}{2} \right) \right) \right. \\ & \left. - \frac{3}{h_1^2} \left( \frac{h_1^2}{4} - \left( \frac{h_1^3}{24} - \frac{y_1^3}{3} \right) \right) (1 - \eta_0^{-1} h_{21}) \right] \psi'(x) \end{aligned} \quad (22)$$

Schematic of the CFRP laminae together with induced stresses, and global and local axes are depicted in Fig. 3.

Given the conventional Euler-Bernoulli beam concept, axial normal stress of the concrete substrate must be expressed as

$$\sigma_{xx}^{(2)} = P_0 + \left[ \frac{1}{h_2} + \frac{6y_2}{h_2^2} (1 + \eta_0^{-1}) \right] \int_{-L/2}^x \psi(\xi) d\xi \quad (23)$$

Integration of the 2D static equilibrium equation relative to  $y_2$  from a particular point to the upper face  $y_2 = h_2/2$  and adopting the associated boundary condition  $\tau_{y_2 x}^{(2)}(-h_1/2) = 0$  writes

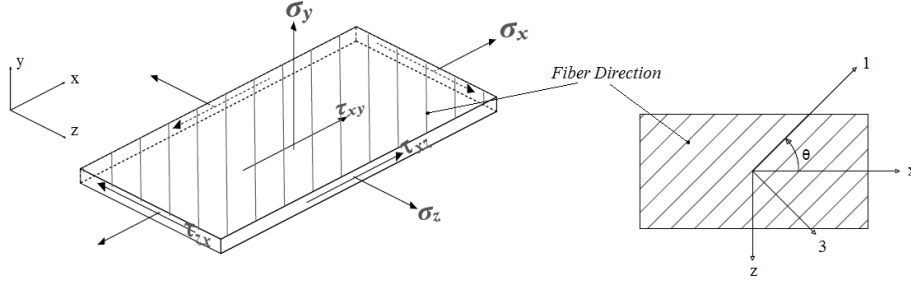


Fig. 3 Schematic of the laminae

$$\tau_{y_2x}^{(2)} = - \left[ \frac{1}{h_2} \left( y_2 + \frac{h_2}{2} \right) + \frac{3}{h_2^2} \left( y_2^2 - \frac{h_2^2}{4} \right) \right] (1 + \eta_0^{-1} h_{21}) \psi(x) \quad (24)$$

Moreover, the normal stress,  $\sigma_{yy}^{(2)}$  of the concrete substrate layer is expressed by the same procedure which reads

$$\sigma_{yy}^{(2)} = \left\{ \frac{1}{h_2} \left[ \frac{1}{2} \left( y_2^2 - \frac{h_2^2}{4} \right) + \frac{h_2}{2} \left( y_2 + \frac{h_2}{2} \right) \right] + \frac{3}{h_2^2} \left[ \frac{1}{3} \left( y_2^3 - \frac{h_2^3}{8} \right) - \frac{h_2^2}{4} \left( y_2 + \frac{h_2}{2} \right) \right] (1 + \eta_0^{-1} h_{21}) \right\} \psi'(x) \quad (25)$$

in which the boundary condition  $\sigma_{yy}^{(2)}(-h_2/2) = 0$  has been used.

## 2.6 Governing equation of the stress functions

The entire strain energy of the CFRP-concrete joint can be determined by integrating the strain energy density (per unit length) relative to  $x$  from  $x = -L/2$  to  $x = +L/2$ . This can be seen to be given by

$$U = b \int_{-\frac{L}{2}}^{\frac{L}{2}} \int_{-\frac{h_1}{2}}^{\frac{h_1}{2}} \left\{ \frac{1}{2} [\sigma_{xx}^{(1)} \varepsilon_{xx}^{(1)} + \sigma_{yy}^{(1)} \varepsilon_{yy}^{(1)}] + \frac{1 + \nu_1}{E_1} (\tau_{y_1x}^{(1)})^2 \right\} dx dy_1 + b \int_{-\frac{L}{2}}^{\frac{L}{2}} \int_{-\frac{h_2}{2}}^{\frac{h_2}{2}} \left\{ \frac{1}{2} [\sigma_{xx}^{(2)} \varepsilon_{xx}^{(2)} + \sigma_{yy}^{(2)} \varepsilon_{yy}^{(2)}] + \frac{1 + \nu_2}{E_2} (\tau_{y_2x}^{(2)})^2 \right\} dx dy_2 \quad (26)$$

In Eq. (26),  $\varepsilon_{xx}^{(1)}$  and  $\varepsilon_{xx}^{(2)}$  are the normal strains of CFRP-composite laminate and concrete substrate layer respectively, which are aligned with  $x$ -direction. For the transversely isotropic CFRP-composite laminate it writes

$$\varepsilon_{xx}^{(1)} = \bar{S}_{11} \sigma_{xx}^{(1)} + \bar{S}_{12} \sigma_{yy}^{(1)} \quad (27)$$

where  $\bar{S}_{ij}$  expressions are terms of transformed compliance matrix, which is the inverse of transformed reduced stiffness matrix; these expressions are functions of the compliance coefficients  $S_{ij}$ , and the fiber orientation,  $\theta$ . Therefore, it reads

$$\bar{S}_{11} = m^4 S_{11} + m^2 n^2 (2S_{12} + S_{66}) + n^2 S_{22} \quad (28)$$

$$\bar{S}_{12} = (m^4 + n^4) S_{12} + m^2 n^2 (S_{11} + S_{22} - S_{66}) \quad (29)$$

where  $m$  and  $n$  are defined as  $m = \cos(\theta)$  and  $n = \sin(\theta)$  and  $\theta$ ,

in degrees, is the angle between the  $x$ -axis and the direction of fibers in CFRP-composite laminate. Moreover

$$S_{11} = \frac{1}{E_1}; \quad S_{12} = -\frac{\nu_{12}}{E_2}; \quad S_{22} = \frac{1}{E_2}; \quad S_{66} = \frac{1}{G_{12}} \quad (30)$$

are the individual compliance coefficients in terms of engineering constants. The Eqs. (28)-(29) can also be expressed in terms of engineering constants of the CFRP-composite laminate. Then the results are

$$\bar{S}_{11} = \left[ m^4 + m^2 n^2 \left( -2\nu_{12} + \frac{E_1}{G_{12}} \right) + n^4 \frac{E_1}{E_2} \right] \left( \frac{1}{E_1} \right) \quad (31)$$

$$\bar{S}_{12} = \left[ m^2 n^2 \left( 1 + \frac{E_1}{E_2} - \frac{E_1}{G_{12}} \right) - (m^4 + n^4) \nu_{12} \right] \left( \frac{1}{E_1} \right) \quad (32)$$

Substitution of the definitions (31) and (32) into Eq. (27) gives

$$\varepsilon_{xx}^{(1)} = \left[ \frac{m^4}{E_1^{(1)}} + m^2 n^2 \left( -2 \frac{\nu_{21}^{(1)}}{E_2^{(1)}} + \frac{1}{G_{12}^{(1)}} \right) + \frac{n^4}{E_2^{(1)}} \right] \sigma_{xx}^{(1)} + \left[ m^2 n^2 \left( \frac{1}{E_1^{(1)}} + \frac{1}{E_2^{(1)}} - \frac{1}{G_{12}^{(1)}} \right) + (m^4 + n^4) \frac{-\nu_{21}^{(1)}}{E_2^{(1)}} \right] \sigma_{yy}^{(1)} \quad (33)$$

As for the isotropic concrete substrate, the normal strain is

$$\varepsilon_{xx}^{(2)} = \frac{\sigma_{xx}^{(2)}}{E^{(2)}} - \nu^{(2)} \frac{\sigma_{yy}^{(2)}}{E^{(2)}} \quad (34)$$

Likewise, the normal strain of CFRP-composite laminate,  $\varepsilon_{yy}^{(1)}$  along  $y$ -axis is

$$\varepsilon_{yy}^{(1)} = \bar{S}_{12} \sigma_{xx}^{(1)} + \bar{S}_{22} \sigma_{yy}^{(1)} \quad (35)$$

where

$$\bar{S}_{22} = n^4 S_{11} + m^2 n^2 (2S_{12} + S_{66}) + m^2 S_{22} \quad (36)$$

In order to express Eq. (36) in engineering constants it writes

$$\bar{S}_{22} = \left[ n^4 + m^2 n^2 \left( -2\nu_{12} + \frac{E_1}{G_{12}} \right) + m^4 \frac{E_1}{E_2} \right] \left( \frac{1}{E_1} \right) \quad (37)$$

Employing Eqs. (32)-(37) into Eq. (35), it can be written

$$\varepsilon_{yy}^{(1)} = \left[ m^2 n^2 \left( \frac{1}{E_1^{(1)}} + \frac{1}{E_2^{(1)}} - \frac{1}{G_{12}^{(1)}} \right) - (m^4 + n^4) \left( \frac{\nu_{21}^{(1)}}{E_2^{(1)}} \right) \right] \sigma_{xx}^{(1)} + \left[ \frac{n^4}{E_1^{(1)}} + m^2 n^2 \left( -2 \frac{\nu_{21}^{(1)}}{E_2^{(1)}} + \frac{1}{G_{12}^{(1)}} \right) + \frac{m^4}{E_2^{(1)}} \right] \sigma_{yy}^{(1)} \quad (38)$$

and the normal strain of concrete substrate layer,  $\varepsilon_{yy}^{(2)}$  is

$$\varepsilon_{yy}^{(2)} = \frac{\sigma_{yy}^{(2)}}{E^{(2)}} - \nu^{(2)} \frac{\sigma_{xx}^{(2)}}{E^{(2)}} \quad (39)$$

The aforementioned complementary strain energy is a functional with respect to the unknown interfacial stress function  $\psi(x)$ .

Based on the theorem of minimum complementary strain energy, the complementary strain energy of the joint regarding the interfacial stress function  $\psi(x)$ , is at the static equilibrium such that  $\delta U = 0$ , where  $\delta$  is the mathematical variational sign with respect to the unknown  $\psi(x)$ . Using the stress resultants, i.e., Eqs. (18), (20), (22), (23), (24) and (25) in Eq. (26), and with setting it equal to zero, yields a 4th-order ordinary differential equation with respect to  $\psi(x)$  as

$$\Psi^{(IV)}(\xi) - 2p\Psi''(\xi) + q^2\Psi(\xi) + t = 0 \quad (40)$$

In Eq. (40)

$$\Psi(\xi) = \Psi\left(\frac{x}{h_1}\right) = -\left(\frac{1}{p_0 h_1}\right) \int_{-L/2}^x \psi(x) dx \quad (41)$$

is a dimensionless stress function; the coefficients  $p = B/-2A$ ,  $q = \sqrt{C/A}$  and  $t = D/A$  are related to the properties of the joint. Moreover, each of the coefficients  $A$ ,  $B$ ,  $C$  and  $D$  are in turn solved by using an efficient code produced by MATLAB.

Mathematically, when  $q > p$ , the solution to Eq. (40) gives

$$\Psi(\xi) = C_1 \cosh(\mu\xi) \cos(\omega\xi) + C_2 \sinh(\mu\xi) \sin(\omega\xi) + t/q^2 \quad (42)$$

where  $\omega = \sqrt{(q-p)/2}$ ;  $\mu = \sqrt{(p+q)/2}$  and  $C_1$  and  $C_2$  are constants. By applying the shear and axial traction-free boundary conditions at  $x = \pm L/2$ ,  $C_1$  and  $C_2$  are obtained and therefore  $\psi(x)$  gives

$$\psi(x) = -P_0 h_1 \frac{d\Psi(\xi)}{dx} = -P_0 [C_1 \mu + C_2 \omega \sinh(\mu x/h_1) \cos(\omega x/h_1) + (-C_1 \omega + C_2 \mu) \cosh(\mu x/h_1) \sin(\omega x/h_1)] \quad (43)$$

In addition, if  $p > q$ , the answer of Eq. (40) yields

$$\Psi(\xi) = C_1 \cosh(\mu\xi) + C_2 \cosh(\omega\xi) + t/q^2 \quad (44)$$

where  $\omega = \sqrt{p - \sqrt{p^2 - q^2}}$ ;  $\mu = \sqrt{p + \sqrt{p^2 - q^2}}$  and  $C_1$  as well as  $C_2$  are two constants. By plugging the shear and axial traction-free boundary conditions at  $x = \pm L/2$ ,  $C_1$  and  $C_2$  are derived and  $\psi(x)$  is organized as

$$\psi(x) = -P_0 h_1 \frac{d\Psi(\xi)}{dx} = -P_0 [C_1 \mu \sinh(\mu x/h_1) + C_2 \omega \sinh(\omega x/h_1)] \quad (45)$$

Correspondingly, the interfacial normal stress  $\phi(x)$ , which was related to  $\psi(x)$  through Eq. (15) can be defined as

$$\phi(x) = -\frac{h_2}{2\eta_0} \psi'(x) \quad (46)$$

### 3. Determining the interfacial stress fields through lamination theory

In this part, the principles of lamination theory applied in a computational MATLAB code have been employed for

finding the interfacial stresses of the joint. The code includes all the mechanical and geometric properties of layers in addition to the external loadings of the joint, combined with the efficient algorithms offered by MATLAB software. The method is based on the lamination theory approach (Herakovich 1998) which describes the linear elastic response of laminated composites. Individual layer properties can be isotropic, orthotropic, or transversely isotropic and in a state of plane stress. In order to develop the stress-strain relationship of the joint layers, 2D constitutive equation for each layer has to be formed as

$$\begin{bmatrix} \sigma_x \\ \sigma_y \\ \tau_{xy} \end{bmatrix} = \begin{bmatrix} \bar{Q}_{11} & \bar{Q}_{12} & \bar{Q}_{16} \\ \bar{Q}_{21} & \bar{Q}_{22} & \bar{Q}_{26} \\ \bar{Q}_{61} & \bar{Q}_{62} & \bar{Q}_{66} \end{bmatrix} \begin{bmatrix} \varepsilon_x \\ \varepsilon_y \\ \gamma_{xy} \end{bmatrix} \quad (47)$$

where  $\bar{Q}_{ij}$  are the transformed reduced stiffness coefficients. The  $[\bar{Q}]$  matrix can be expressed as

$$[\bar{Q}] = [T]^{-1}[Q][R][T][R]^{-1} \quad (48)$$

in which  $[T]$  is termed the transformation matrix and is defined as

$$[T] = \begin{bmatrix} \cos^2 \theta & \sin^2 \theta & 2 \sin \theta \cos \theta \\ \sin^2 \theta & \cos^2 \theta & -2 \sin \theta \cos \theta \\ -\sin \theta \cos \theta & \sin \theta \cos \theta & \cos^2 \theta - \sin^2 \theta \end{bmatrix} \quad (49)$$

and  $[R]$  is the Reuter matrix. The inverse of the compliance matrix is  $[Q]$ , the stiffness matrix, i.e.,  $[Q] = [S]^{-1}$ . The compliance matrix  $[S]$ , can be expressed in terms of engineering constants of the material which writes

$$[S] = \begin{bmatrix} S_{11} & S_{12} & S_{16} \\ S_{21} & S_{22} & S_{26} \\ S_{61} & S_{62} & S_{66} \end{bmatrix} = \begin{bmatrix} 1/E_1 & -\nu_{12}/E_1 & 0 \\ -\nu_{12}/E_1 & 1/E_2 & 0 \\ 0 & 0 & 1/G_{12} \end{bmatrix} \quad (50)$$

To determine the strains in Eq. (47), it reads

$$\begin{Bmatrix} \varepsilon_x \\ \varepsilon_y \\ \gamma_{xy} \end{Bmatrix} = \begin{Bmatrix} \varepsilon_x^0 \\ \varepsilon_y^0 \\ \gamma_{xy}^0 \end{Bmatrix} + z \begin{Bmatrix} \kappa_x \\ \kappa_y \\ \kappa_{xy} \end{Bmatrix} \quad (51)$$

Eq. (51) expresses the total strains  $\varepsilon$ , at any  $z$ -location of the laminate, in terms of midplane strains  $\varepsilon^0$ , and the curvatures  $\kappa$ ;  $z$  is the point of interest at which stresses and strains are calculated and is measured from the midplane. It is comprehended that the total strains are the sum of midplane strains and the strains associated with curvature, which is the fundamental equation of lamination theory. The midplane strains and curvatures can be considered using the equation

$$\begin{Bmatrix} \varepsilon_x^0 \\ \varepsilon_y^0 \\ \gamma_{xy}^0 \\ \kappa_x \\ \kappa_y \\ \kappa_{xy} \end{Bmatrix} = \begin{bmatrix} [A] & [B] \\ [B] & [D] \end{bmatrix} \begin{Bmatrix} N_x \\ N_y \\ N_{xy} \\ M_x \\ M_y \\ M_{xy} \end{Bmatrix} \quad (52)$$

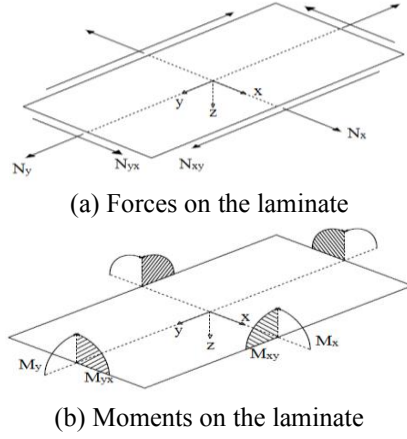


Fig. 4 Schematic of the actions

where  $[A]$ ,  $[B]$  and  $[D]$  matrices are termed the extensional, coupling and bending stiffness matrices, respectively, and are defined as

$$\begin{cases} A_{ij} = \sum_{k=1}^n [\bar{Q}_{ij}]_k t_k & i = 1,2,6 \\ B_{ij} = 1/2 \sum_{k=1}^n [\bar{Q}_{ij}]_k t_k^2 & i = 1,2,6 \\ D_{ij} = 1/3 \sum_{k=1}^n [\bar{Q}_{ij}]_k t_k^3 & i = 1,2,6 \end{cases} \quad (53)$$

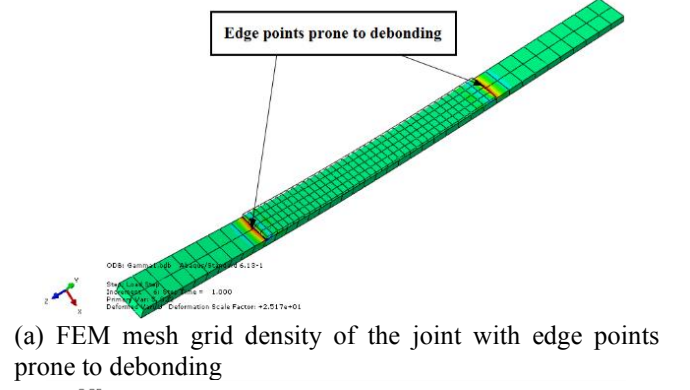
where  $t_k$  is the thickness of  $k$ -th layer. The resulting forces and moments are expressed as follows.  $N_x$  and  $N_y$  are normal forces per unit length;  $N_{xy}$  is the shear force per unit length;  $M_x$  and  $M_y$  are bending moments per unit length and  $M_{xy}$  is the twisting moment per unit length. Fig. 4 (a)-(b) illustrates the in-plane resultant forces and moments per unit length, respectively.

Therefore, if midplane strains, laminate curvatures, and stacking sequence of the composite laminate are known, strains and stresses at any  $z$ -location can be determined directly from Eq. (47).

#### 4. Validating example

To validate the present analytic solutions of shear and normal interfacial stress fields along the bondline, the authors examined an isotropic bimaterial steel-aluminum beam. The beam is assumed to be under the action of uniform axial tension,  $P_0$  which is applied at both ends of the tension bar, i.e., the aluminum substrate layer (Fig. 5). In this case, the strengthened length in the model is  $L/2 = 20$  mm. Other geometric and mechanical properties are as follows:  $h_1=2$  mm,  $E_1=200$  GPa and  $\nu_1=0.29$  for the steel reinforcing cover;  $h_2=4$  mm,  $E_2=70$  GPa and  $\nu_2=0.34$  for the aluminum substrate layer. The given  $P_0$  is assumed to be 1 MPa.

The accuracy of stress fields in the present model relies on the computational process of solving the 4th-order ordinary differential equation (Eq. (40)). Applying the principles of lamination theory, a MATLAB code was instrumented to compare the results obtained from the present model and those of Wu and Jenson's (2014). This code also serves to illustrate the behavior of varying free-edge normal and shear interfacial stresses along the



(a) FEM mesh grid density of the joint with edge points prone to debonding

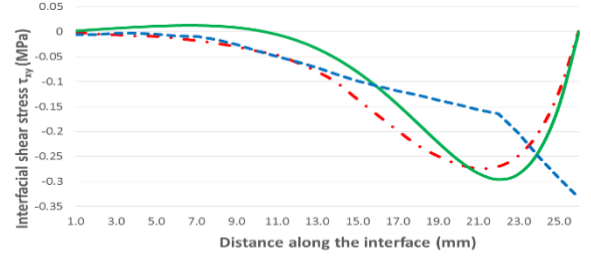
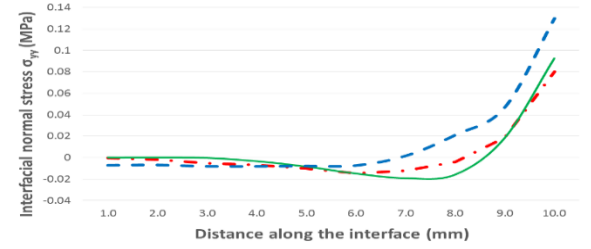

 (b) Shear stress field along the interface ( $\tau$ )

 (c) Normal stress field along the interface ( $\sigma$ )

Fig. 6 Comparison of interfacial shear and normal stresses proposed by the present model with those of FEM

bondline. Owing to the presence of stress singularities, the stresses tend to increase drastically at the free-edges of bimaterials. The results of the analysis, shown in Fig. 5 (b)-(c), suggest good conformity with the present findings in the literature. Compared to normal interfacial stress with the peak value of 0.093 (MPa), high interfacial shear stress with the peak value of -0.296 (MPa) mainly contributes to the debonding failure of the joint.

To further verify the proposed analytic solution, FEM based on commercial finite element analysis software package ABAQUS 6.13-1 was implemented. During the numerical analysis of the abovementioned beam in the case of plane-stress state, 8-node linear elements (C3D8R) and exclusively hexahedral mesh of size 0.5 mm were employed. A nonuniform distribution of elements along the bondline was used to precisely capture the trend of singular stress variations along the bondline as shown in Fig. 6.

It can be observed that interfacial stresses are highly localized at the near-free end of the bondline. Obviously, the interfacial shear stresses predicted by the present

Table 1 The mechanical properties of the concrete layer

$E_1$ (GPa)	Axial modulus	$G_{12}$ (GPa)	Shear modulus	$\nu_{12}$ Poisson's ratio	$f'_c$ (MPa)	Concrete cylinder strength
30		10.5		0.2		40

Table 2 The mechanical properties of the CFRP laminate

Type	$E_1$ (GPa)	$E_2=E_3$ (GPa)	$G_{12}=G_{13}$ (GPa)	$G_{23}$ (GPa)	$\nu_{12}=\nu_{13}$	$\nu_{23}$
T300/5208	132	10.8	5.65	3.38	0.24	0.59

Table 3 The mechanical and geometric properties of materials with respect to different values of  $\alpha$ 

$\alpha$	$l_1$	$l_2$	$h_1$	$h_2$	$b$	$P_0$	Stacking Sequence
1	400	400	2	10	10	20	[0/90]
1.5	266	400	2	10	10	20	[0/90]
2	200	400	2	10	10	20	[0/90]
3	134	400	2	10	10	20	[0/90]

$l$  and  $h$  values are in mm;  $P_0$  values are in MPa

lamination theory approach exactly satisfy the shear-free BCs in the joint as required by the theoretical formulation. Even though the normal stresses adopt the very similar varying trend for the FEM along the bondline, shear stresses are not zero at the very ending edges of the cover layer, which is because of the singular state of such stresses; however the peak values happen to correspond with those of proposed method.

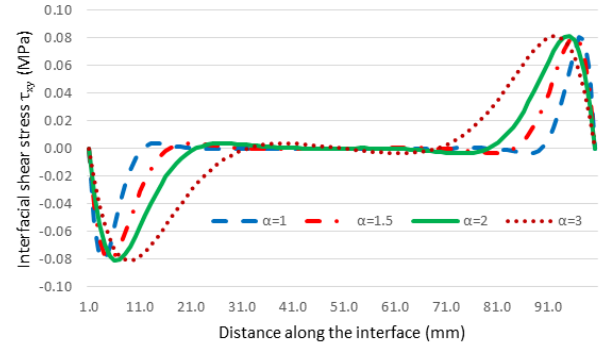
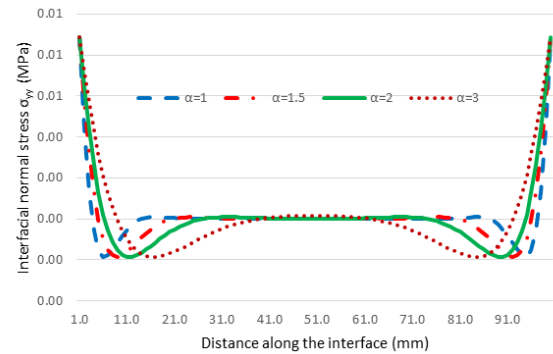
## 5. Scaling analysis of interfacial shear and normal stresses

This section triggers evaluating the effects of geometric and mechanical changes of adherents on the interfacial shear and normal stress distributions along the bondline in the beam under study (Fig. 1(a)). The mechanical properties of concrete substrate layer and CFRP-composite laminate are given in Tables 1-2, respectively. It is noted that the elastic modulus of concrete and CFRP are kept constant throughout this section.

Furthermore, an inclusive computational MATLAB code was designed to study the dependencies of such stress fields upon the mechanical/geometric parameters. Some parameters are introduced as follows:

Define  $\alpha = l_2/l_1$  as the length ratio where  $l_2$  is the length of concrete substrate layer and  $l_1$  is the CFRP-composite laminate length. Table 3 presents the details of geometric dimensions and mechanical properties of materials used in the analysis. Four length ratios ( $\alpha = 1, 1.5, 2, 3$ ) were implemented in this section.

Fig. 7 (a)-(b) plots the variations of interfacial shear and normal stresses along the CFRP-concrete bondline with respect to different values of  $\alpha$ . It can be seen that high interfacial shear and normal stress concentrations occur near the free edges of the adherents, i.e., the boundary layer region, while the points close to mid-span (the central region) are almost stress free. Moreover, a change in the

(a) Interfacial shear stress ( $\tau$ )(b) Interfacial normal stress ( $\sigma$ )Fig. 7 Variations of interfacial stress fields along the interface with respect to different values of  $\alpha$ Table 4 The mechanical and geometric properties of materials with respect to different values of  $\beta$ 

$\alpha$	$\beta$	$l_1$	$l_2$	$h_1$	$h_2$	$b$	$P_0$	Stacking Sequence
2	2.5	200	400	4	10	10	20	[0/90]
2	5	200	400	2	10	10	20	[0/90]
2	10	200	400	1	10	10	20	[0/90]

$l$  and  $h$  values are in mm;  $P_0$  values are in MPa

length ratio does not substantially influence the interfacial stress variations.

Another parameter to define is  $\beta = h_2/h_1$  as the thickness ratio, where  $h_2$  is the thickness of concrete layer and  $h_1$  is the CFRP laminate thickness. Table 4 reports the detailed properties of concrete layer and CFRP laminate with respect to different values of  $\beta$ . Furthermore, Fig. 8 (a)-(b), respectively depicts the trend of interfacial shear and normal stress variations along the CFRP-concrete interface. It is discerned that as the thickness ratio increases, i.e., decrease in the CFRP laminate thickness, the peak shear and normal stresses decline. In other words, thicker reinforcing patches produce larger stresses on the interface.

The third parameter to investigate is the depth ratio,  $\gamma = h_2/b$ , where  $h_2$  is the thickness of concrete layer and  $b$  is the width of joint. The properties of materials utilized in this part for various values of  $\gamma$  are provided in Table 5.

Variations of stresses along the interface for different values of  $\gamma$  are shown in Fig. 9 (a)-(b). Along with the increment in depth ratio, both interfacial shear and normal stresses decrease at free edges. Given the rest of parameters

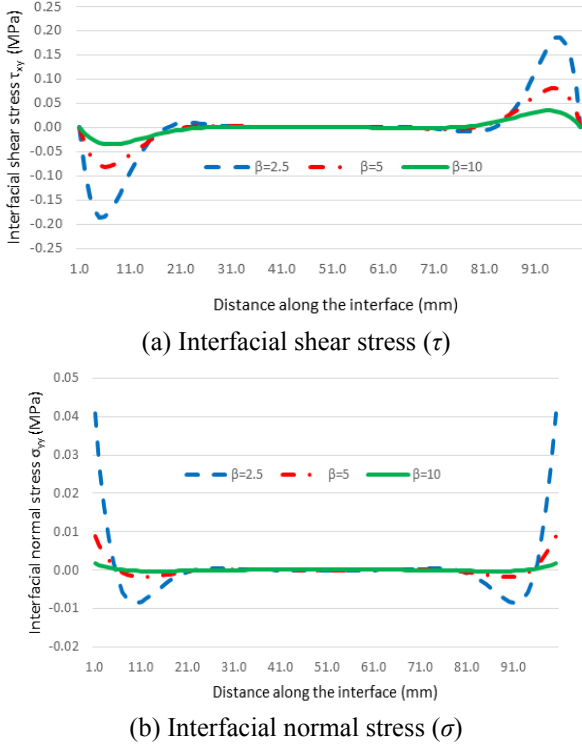


Fig. 8 Variations of interfacial stress fields along the interface with respect to different values of  $\beta$

Table 5 The mechanical and geometric properties of materials with respect to different values of  $\gamma$

$\alpha$	$\gamma$	$l_1$	$l_2$	$h_1$	$h_2$	$b$	$P_0$	Stacking Sequence
2	1.5	200	400	2	15	10	20	[0/90]
2	2	200	400	2	20	10	20	[0/90]
2	3	200	400	2	30	10	20	[0/90]

$l$  and  $h$  values are in mm;  $P_0$  values are in MPa

be fixed, it is concluded that interfacial stresses produce lower values for deep concrete prisms strengthened with CFRP laminates. As it is illustrated in Fig. 9, akin to previous figures, the shear stresses satisfy all the shear-free boundary conditions at the adherents' free edges.

To examine the dependency of stresses upon the elastic modulus of adherents, three modulus ratios,  $\varphi = E_f/E_c$ , ( $\varphi = 2, 4, 6$ ) are defined as the fourth parameter.  $E_f$  and  $E_c$  are respectively the Young's moduli of CFRP composite and concrete. Table 6 summarizes the properties of materials utilized in this part. The effect of  $\varphi$  on the stress fields are plotted in Fig. 10 (a)-(b). It should be noted that the variation in  $\varphi$  stems from the change in elastic modulus of concrete. It is then comprehended, according to Fig. 10, that a change in  $E_f$ , does not considerably affect the stress field distributions.

The fifth parameter to probe, is the CFRP fiber orientation  $\theta$ , and the stacking sequence. Firstly, four stacking sequences [0/0], [0/90], [90/0] and [90/90] were adopted. Fig. 11 (a)-(b) sketches the way interfacial shear and normal stresses vary with respect to different stacking sequences. It is perceived that the [90/90] sequence

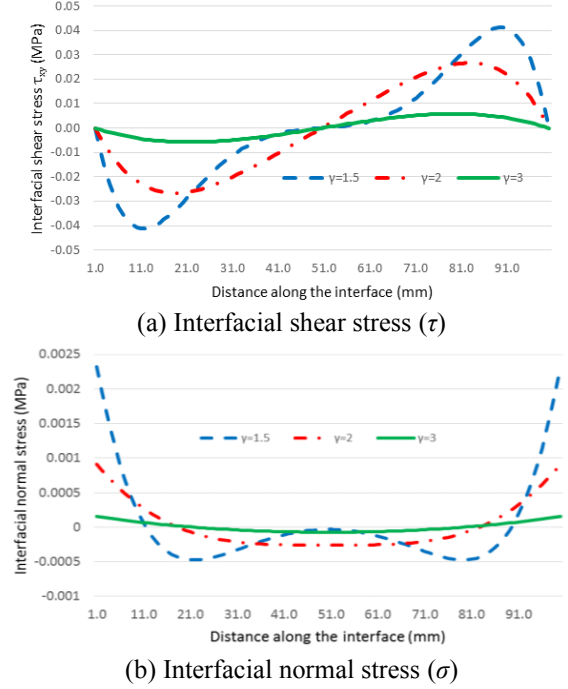


Fig. 9 Variations of interfacial stress fields along the interface with respect to different values of  $\gamma$

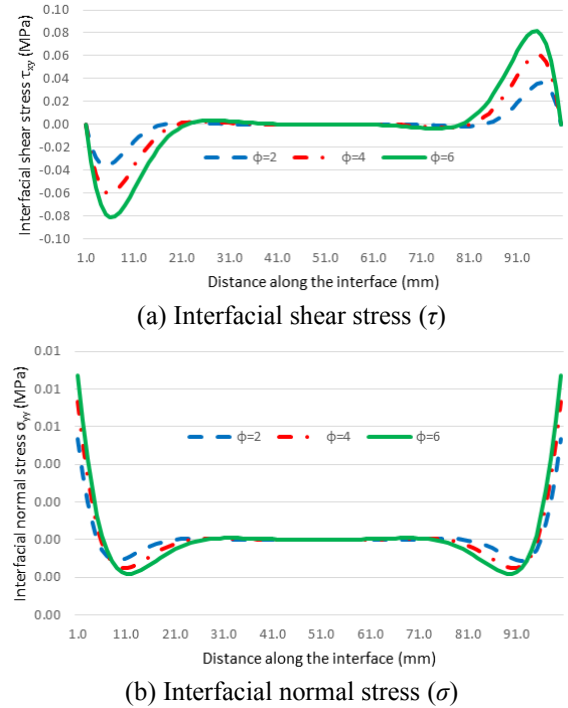


Fig. 10 Variations of interfacial stress fields along the interface with respect to different values of  $\varphi$

Table 6 The mechanical and geometric properties of materials with respect to different values of  $\varphi$

$\alpha$	$\beta$	$\gamma$	$\varphi$	$l_1$	$l_2$	$h_1$	$h_2$	$b$	$P_0$	Stacking Sequence
2	5	1	2	200	400	2	10	10	20	[0/90]
2	5	1	4	200	400	2	10	10	20	[0/90]
2	5	1	6	200	400	2	10	10	20	[0/90]

$l$  and  $h$  values are in mm;  $P_0$  values are in MPa

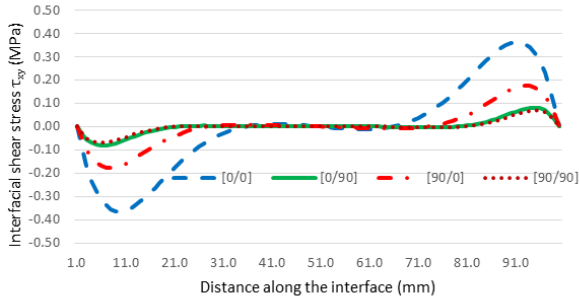
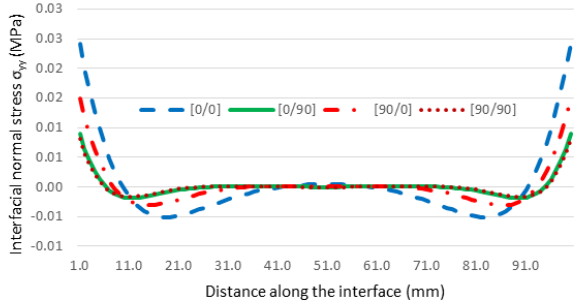
(a) Interfacial shear stress ( $\tau$ )(b) Interfacial normal stress ( $\sigma$ )

Fig. 11 Variations of interfacial stress fields along the interface with respect to different stacking sequences

Table 7 The mechanical and geometric properties of materials for  $\theta$  dependency evaluation

$\alpha$	$\beta$	$\gamma$	$\varphi$	$l_1$	$l_2$	$h_1$	$h_2$	$b$	$P_0$
2	5	1	4.4	200	400	2	10	10	20
2	5	1	4.4	200	400	2	10	10	20
2	5	1	4.4	200	400	2	10	10	20

$l$  and  $h$  values are in mm;  $P_0$  values are in MPa

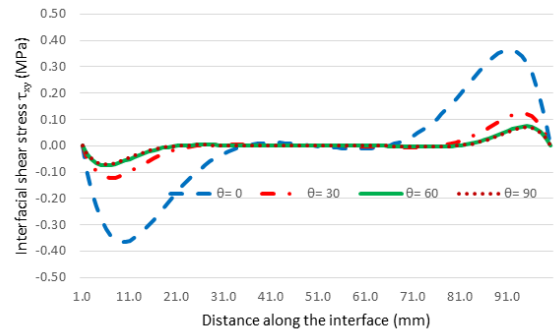
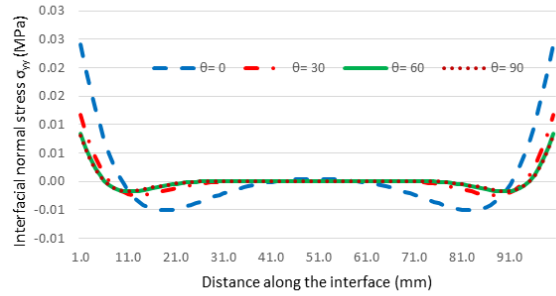
produces lower interfacial stresses in comparison to others, hence it is more favorable in designing the joint.

The same procedure was reiterated with stackings [0/0], [0/45], [45/0] and [45/45] and both shear and normal stresses in [45/45] were lower. It was concluded that amongst the aforementioned stacking sequences,  $[\theta/\theta]$  would result in lower peak values of stress. Secondly, a comparison was conducted to find out the lowest maximum stress values with  $\theta$  from 0 to 90 degrees at every 15 degrees of intervals. The presumed values of properties are given in Table 7.

Fig. 12 (a)-(b) implies that as the fiber orientation,  $\theta$  increases from its initial value, i.e., from  $\theta = 0$  to  $\theta = 90$ , the interfacial shear and normal stresses tend to decrease in the boundary layer region.

## 6. Conclusions

This paper aimed at proposing a systematic approach on determining the prominent interfacial normal and shear stresses of a CFRP-concrete bonded joint. Accordingly, two normal and shear stress functions were introduced using the semi-analytic stress-function variational approach. The two stress functions satisfy all the traction boundary conditions

(a) Interfacial shear stress ( $\tau$ )(b) Interfacial normal stress ( $\sigma$ )Fig. 12 Variations of interfacial stress fields along the interface with respect to different  $[\theta/\theta]$  stacking sequences

including the shear-free condition at free edges of the adherents, which has been normally neglected in the majority of joint models within the literature. Applying the complementary strain energy theory, the governing ordinary differential equation was determined. A concise MATLAB code was then designed by implementing the highly robust and efficient lamination theory approach in order to determine the entire stress field throughout the examined joint. It is capable of taking into account different types of loading, stacking sequence, material properties, orientations and the thickness of layers. Furthermore, a scaling analysis was conducted to analyze the effective issues on the interfacial stresses using this code. The following conclusions were drawn:

- Intense stresses at the interface occur in the vicinity of adherent free ends (also termed the boundary layer region), while the central region (close to mid-span) is almost stress-free.
- Shear stresses satisfy all the shear-free boundary conditions at the free ends of adherents for all types of geometric configurations.
- The change in length ratio (concrete layer to CFRP laminate length ratio) does not considerably affect the peak interfacial stress values.
- As compared with the maximum interfacial normal stresses, debonding failure of the joint in all configurations is attributable to the high interfacial shear stresses.
- As the thickness ratio (concrete layer to CFRP laminate thickness ratio) increases, both interfacial shear and normal stresses tend to decrease.
- The depth ratio (concrete layer to joint width ratio) has an inverse relation with the interfacial stress values.

- Taking into account the dependency of interfacial stresses on the elastic modulus ratio (CFRP laminate to concrete layer modulus ratio), the elastic modulus of concrete has more influence on the stresses rather than that of CFRP.
- Among different values for  $\theta$ , from 0 to 90 degrees in  $[\theta / \theta]$  stacking,  $\theta=0$  generates higher interfacial shear and normal stresses; in addition, as  $\theta$  increases, the peak stress values decrease such that  $\theta=90$  produces the lowest stress values.

## Acknowledgement

The authors would like to appreciate the civil engineering faculty members in Babol Noshirvani University of Technology of Iran, who kindly examined the research and suggested useful comments and modifications.

## References

- Ali, M.M., Oehlers, D.J. and Bradford, M.A. (2001), "Shear peeling of steel plates bonded to tension faces of RC beams", *J. Struct. Eng.*, **127**(12), 1453-1459. [https://doi.org/10.1061/\(ASCE\)0733-9445\(2001\)127:12\(1453\)](https://doi.org/10.1061/(ASCE)0733-9445(2001)127:12(1453)).
- Ali, M.M., Oehlers, D.J. and Bradford, M.A. (2002), "Interaction between flexure and shear on the debonding of RC beams retrofitted with compression face plates", *Adv. Struct. Eng.*, **5**(4), 223-230. <https://doi.org/10.1260/136943302320974590>.
- American Concrete Institute (ACI) (2008), Guide for the Design and Construction of Externally Bonded FRP Systems for Strengthening Concrete Structure, ACI 440.2R-08, Farmington Hills, MI, USA.
- Beer, F., Johnston, E.R., Dewolf, J.T. and Mazurek, D.F. (2009), *Mechanics of Materials*, 5th Edition, McGraw Hill, New York, NY, USA.
- CNR-DT 200 (2004), Guide for the Design and Construction of Externally Bonded FRP Systems for Strengthening.
- Concrete Society (2004), Design Guidance for Strengthening Concrete Structures with Fiber Composite Materials, Concrete Society Technical Rep. No. 55, 2nd Ed., Surrey, U.K.
- Dogan, A.B. and Anil, O. (2010), "Nonlinear finite element analysis of effective CFRP bonding length and strain distribution along concrete-CFRP interface", *Comput. Concrete*, **7**(5), 437-453. <https://doi.org/10.12989/cac.2010.7.5.437>.
- Hashemi, S.H., Maghsoudi, A.A. and Rahgozar, R. (2008), "Flexural ductility of reinforced HSC beams strengthened with CFRP sheets", *Struct. Eng. Mech.*, **30**(4), 403-426. <http://dx.doi.org/10.12989/sem.2008.30.4.403>.
- Herakovich, C.T. (1998), *Mechanics of Fibrous Composites*, John Wiley & Sons, Inc.
- Hosseini, A. and Mostofinejad, D. (2013), "Experimental investigation into bond behavior of CFRP sheets attached to concrete using EBR and EBROG techniques", *Compos. Part B: Eng.*, **51**, 130-139. <https://doi.org/10.1016/j.compositesb.2013.03.003>.
- International Federation for Structural Concrete (fib) (2001), "Externally bonded FRP reinforcement for RC structures", Technical Report, Task Group 9.3, Bulletin No. 14, Lausanne, Switzerland.
- Japan Society of Civil Engineers (JSCE) (2001), "Recommendations for upgrading of concrete structures with use of continuous fiber sheets", Concrete Engineering Series, 41, English Version, Tokyo.
- Karbhari, V.M. and Abanilla, M.A. (2007), "Design factors, reliability, and durability prediction of wet layup carbon/epoxy used in external strengthening", *Compos. Part B: Eng.*, **38**(1), 10-23. <https://doi.org/10.1016/j.compositesb.2006.06.001>.
- Kassapoglou, C. (1990), "Determination of interlaminar stresses in composite laminates under combined loads", *J. Reinf. Plast. Compos.*, **9**(1), 33-58. <https://doi.org/10.1177/073168449000900103>.
- Kassapoglou, C. and Lagace, P.A. (1986), "An efficient method for the calculation of interlaminar stresses in composite materials", *J. Appl. Mech.*, **53**(4), 744-750.
- Kassapoglou, C. and Lagace, P.A. (1987), "Closed form solutions for the interlaminar stress field in angle-ply and cross-ply laminates", *J. Compos. Mater.*, **21**(4), 292-308. <https://doi.org/10.1177/002199838702100401>.
- Kaw, A.K. (2006), *Mechanics of Composite Materials*, Second Edition, Taylor & Francis Group, LLC.
- Khan, U., Al-Osta, M.A. and Ibrahim, A. (2017), "Modeling shear behavior of reinforced concrete beams strengthened with externally bonded CFRP sheets", *Struct. Eng. Mech.*, **61**(1), 125-142. <https://doi.org/10.12989/sem.2017.61.1.125>.
- Lin, H.X., Lu, J.Y. and Xu, B. (2017), "Numerical approach to fracture behavior of CFRP/concrete bonded interfaces", *Comput. Concrete*, **20**(3), 291-295. <https://doi.org/10.12989/cac.2017.20.3.291>.
- MATLAB Documentation (2011), General Release Notes, Release 2011a, Version 7.12.0.635.
- Oehlers, D.J. and Moran, J.P. (1990), "Premature failure of externally plated reinforced concrete beams", *J. Struct. Eng.*, **116**(4), 978-995. [https://doi.org/10.1061/\(ASCE\)0733-9445\(1990\)116:4\(978\)](https://doi.org/10.1061/(ASCE)0733-9445(1990)116:4(978)).
- Oehlers, D.J., Park, S.M. and Ali, M.M. (2003), "A structural engineering approach to adhesive bonding longitudinal plates to RC beams and slabs", *Compos. Part A: Appl. Sci. Manuf.*, **34**(9), 887-897. [https://doi.org/10.1016/S1359-835X\(03\)00153-2](https://doi.org/10.1016/S1359-835X(03)00153-2).
- Pagano, N.J. (1978), "Free edge stress fields in composite laminates", *Int. J. Solid. Struct.*, **14**(5), 401-406. [https://doi.org/10.1016/0020-7683\(78\)90021-5](https://doi.org/10.1016/0020-7683(78)90021-5).
- Pagano, N.J. (1978), "Stress fields in composite laminates", *Int. J. Solid. Struct.*, **14**(5), 385-400. [https://doi.org/10.1016/0020-7683\(78\)90020-3](https://doi.org/10.1016/0020-7683(78)90020-3).
- Pattabhi, G., Santosh, S., Latha, I.B., Rao, M.V. and Kumar, C.A. (2012), "Analysis of adhesively bonded double lap joint in laminated FRP composites subjected to longitudinal loading", *Int. J. Eng. Sci. Adv. Technol.*, **2**(2), 307-316.
- Pipes, R.B. and Pagano, N.J. (1974), "Interlaminar stresses in composite laminates-an approximate elasticity solution", *J. Appl. Mech.*, **41**(3), 668-672. <https://doi.org/10.1115/1.3423368>.
- Puppo, A.H. and Evensen, H.A. (1970), "Interlaminar shear in laminated composites under generalized plane stress", *J. Compos. Mater.*, **4**(2), 204-220. <https://doi.org/10.1177/002199837000400206>.
- Smith, S.T. and Teng, J.G. (2002), "FRP-strengthened RC beams. I: review of debonding strength models", *Eng. Struct.*, **24**(4), 385-395. [https://doi.org/10.1016/S0141-0296\(01\)00105-5](https://doi.org/10.1016/S0141-0296(01)00105-5).
- Smith, S.T. and Teng, J.G. (2002), "FRP-strengthened RC beams. II: assessment of debonding strength models", *Eng. Struct.*, **24**(4), 397-417. [https://doi.org/10.1016/S0141-0296\(01\)00106-7](https://doi.org/10.1016/S0141-0296(01)00106-7).
- Smith, S.T. and Teng, J.G. (2003), "Shear-bending interaction in debonding failures of FRP-plated RC beams", *Adv. Struct. Eng.*, **6**(3), 183-199. <https://doi.org/10.1260/136943303322419214>.
- Tang, S. (1975), "A boundary layer theory-Part I: Laminated composites in plane stress", *J. Compos. Mater.*, **9**(1), 33-41. <https://doi.org/10.1177/002199837500900104>.

- Tang, S. and Levy, A. (1975), "A boundary layer theory-part II: extension of laminated finite strip", *J. Compos. Mater.*, **9**(1), 42-52. <https://doi.org/10.1177/002199837500900105>.
- Teng, J.G., Smith, S.T., Yao, J. and Chen, J.F. (2003), "Intermediate crack-induced debonding in RC beams and slabs", *Constr. Build. Mater.*, **17**(6-7), 447-462. [https://doi.org/10.1016/S0950-0618\(03\)00043-6](https://doi.org/10.1016/S0950-0618(03)00043-6).
- Touati, M., Tounsi, A. and Benguediab, M. (2015), "Effect of shear deformation on adhesive stresses in plated concrete beams: Analytical solutions", *Comput. Concrete*, **15**(3), 337-355. <https://doi.org/10.12989/cac.2015.15.3.337>.
- Wu, X.F. and Dzenis, Y.A. (2005), "Experimental determination of probabilistic edge-delamination strength of a graphite-fiber/epoxy composite", *Compos. Struct.*, **70**(1), 100-108. <https://doi.org/10.1016/j.compstruct.2004.08.016>.
- Wu, X.F. and Jenson, R.A. (2011), "Stress-function variational method for stress analysis of bonded joints under mechanical and thermal loads", *Int. J. Eng. Sci.*, **49**(3), 279-294. <https://doi.org/10.1016/j.ijengsci.2010.11.005>.
- Wu, X.F. and Jenson, R.A. (2014), "Semianalytic stress-function variational approach for the interfacial stresses in bonded joints", *J. Eng. Mech.*, **140**(11), 04014089. [https://doi.org/10.1061/\(ASCE\)EM.1943-7889.0000803](https://doi.org/10.1061/(ASCE)EM.1943-7889.0000803).